The Astronomical Journal, 151:82 (12pp), 2016 March doi:10.3847/0004-6256/151/3/82

DETAILED CHEMICAL ABUNDANCES IN THE *r*-PROCESS-RICH ULTRA-FAINT DWARF GALAXY RETICULUM 2*

Ian U. Roederer[1,2], Mario Mateo[1], John I. Bailey III[1], Yingyi Song[1], Eric F. Bell[1], Jeffrey D. Crane[3], Sarah Loebman[1], David L. Nidever[1,4,5], Edward W. Olszewski[5], Stephen A. Shectman[3], Ian B. Thompson[3], Monica Valluri[1], and Matthew G. Walker[6]

[1] Department of Astronomy, University of Michigan, 1085 S. University Ave., Ann Arbor, MI 48109, USA; iur@umich.edu
[2] Joint Institute for Nuclear Astrophysics and Center for the Evolution of the Elements (JINA-CEE), USA
[3] Carnegie Observatories, 813 Santa Barbara St., Pasadena, CA 91101, USA
[4] Large Synoptic Survey Telescope, 950 North Cherry Ave., Tucson, AZ 85719, USA
[5] Steward Observatory, 933 North Cherry Ave, Tucson, AZ 85719, USA
[6] McWilliams Center for Cosmology, Department of Physics, Carnegie Mellon University, 5000 Forbes Ave., Pittsburgh, PA 15213, USA
Received 2015 December 21; accepted 2016 January 15; published 2016 February 29

ABSTRACT

The ultra-faint dwarf (UFD) galaxy Reticulum 2 (Ret 2) was recently discovered in images obtained by the Dark Energy Survey. We have observed the four brightest red giants in Ret 2 at high spectral resolution using the Michigan/*Magellan* Fiber System. We present detailed abundances for as many as 20 elements per star, including 12 elements heavier than the Fe group. We confirm previous detection of high levels of *r*-process material in Ret 2 (mean [Eu/Fe] $= +1.69 \pm 0.05$) found in three of these stars (mean [Fe/H] $= -2.88 \pm 0.10$). The abundances closely match the *r*-process pattern found in the well-studied metal-poor halo star CS 22892–052. Such *r*-process-enhanced stars have not been found in any other UFD galaxy, though their existence has been predicted by at least one model. The fourth star in Ret 2 ([Fe/H] $= -3.42 \pm 0.20$) contains only trace amounts of Sr ([Sr/Fe] $= -1.73 \pm 0.43$) and no detectable heavier elements. One *r*-process enhanced star is also enhanced in C (natal [C/Fe] $\approx +1.1$). This is only the third such star known, which suggests that the nucleosynthesis sites leading to C and *r*-process enhancements are decoupled. The *r*-process-deficient star is enhanced in Mg ([Mg/Fe] $= +0.81 \pm 0.14$), and the other three stars show normal levels of α-enhancement (mean [Mg/Fe] $= +0.34 \pm 0.03$). The abundances of other α and Fe-group elements closely resemble those in UFD galaxies and metal-poor halo stars, suggesting that the nucleosynthesis that led to the large *r*-process enhancements either produced no light elements or produced light-element abundance signatures indistinguishable from normal supernovae.

Key words: galaxies: dwarf – galaxies: individual (Reticulum 2) – nuclear reactions, nucleosynthesis, abundances – stars: abundances

Supporting material: machine-readable tables

1. INTRODUCTION

Images obtained by the Dark Energy Survey (DES; Diehl et al. 2014) have recently revealed 17 new faint Milky Way satellite candidates toward the general direction of the Magellanic Clouds (Bechtol et al. 2015; Drlica-Wagner et al. 2015; Koposov et al. 2015a). One of these, Reticulum 2 (Ret 2), is the nearest (≈30 kpc) ultra-faint dwarf galaxy (UFD; $M_V = -2.7$) to the Milky Way in the southern hemisphere. Reconnaissance spectroscopy of Ret 2 (Koposov et al. 2015b; Simon et al. 2015; Walker et al. 2015) have confirmed Ret 2 has low mean metallicity ([Fe/H] $= -2.6$), a significant metallicity dispersion ($\sigma_{\rm [Fe/H]} \approx 0.5$), and a high mass-to-light ratio ($\gtrsim$500 in solar units). Though located relatively close to the Large Magellanic Cloud, it remains unclear whether Ret 2 was originally a satellite of the Magellanic system (Koposov et al. 2015b). No H I has been detected in Ret 2 (Westmeier et al. 2015). Geringer-Sameth et al. (2015) report a possible gamma-ray signal detection toward Ret 2 that may be consistent with dark matter annihilation.

Ji et al. (2015a) presented the first abundances derived from high-resolution spectroscopy of nine of the brightest stars in Ret 2. Their startling finding is that seven of these nine stars are highly enhanced in material produced by the rapid neutron-capture process (*r*-process). This is remarkable on several levels.

First, no previous studies of dozens of stars in nine UFD galaxies have revealed large enhancements of heavy elements produced by *r*-process nucleosynthesis (Koch et al. 2008; Feltzing et al. 2009; Frebel et al. 2010, 2014; Norris et al. 2010a, 2010b; Simon et al. 2010; Gilmore et al. 2013; Koch et al. 2013; Ishigaki et al. 2014a; Koch & Rich 2014; Roederer & Kirby 2014; François et al. 2015; Ji et al. 2015b). Typically, elements produced by neutron-capture (*n*-capture) reactions are difficult to detect in the UFD galaxies, and their abundances are among the lowest known in any stars.

Second, stars with such high levels of *r*-process material ([Eu/Fe] $> +1$ and [Ba/Eu] < 0; hereafter known as *r*-II stars, Christlieb et al. 2004) are relatively rare among the metal-poor stars in the solar neighborhood (~3%; Barklem et al. 2005). About 20 *r*-II stars are known, and all are located in the halo, with the exception of one star in UMi (Shetrone et al. 2001; Sadakane et al. 2004; Aoki et al. 2007b) and one in the Milky Way bulge (Johnson et al. 2013). Until now, none of the stars in the *r*-II class have been physically associated with each

* This paper includes data gathered with the 6.5 m *Magellan* Telescopes located at Las Campanas Observatory, Chile.

other, and finding a galaxy teeming with such stars is unprecedented.

Third, there have been few opportunities to test the role that environment plays in the formation of *r*-II stars and *r*-process nucleosynthesis more generally. Ji et al. (2015a) assumed that UFD galaxies like Ret 2 formed in minihalos with $\sim 10^6\ M_\odot$ of H (e.g., Bromm & Larson 2004). Ji et al. (2015a) concluded that the *r*-process material originated in a single neutron-star merger (e.g., Goriely et al. 2011; Ramirez-Ruiz et al. 2015) or any other rare site with high *r*-process yields ($\sim 10^{-4.5}\ M_\odot$ of Eu per event). The amount of *r*-process material required scales with the assumed H mass of the minihalo. The dilution of metals into H may not be uniform across the galaxy, and all *r*-process material may not be incorporated into stars, but this sets a lower limit on the amount of *r*-process material necessary.

Previous attempts to identify the astrophysical source(s) of the *r*-process have focused on characterizing the *r*-process abundance pattern in detail (e.g., Sneden et al. 1996, 2003; Hill et al. 2002; Christlieb et al. 2004; Frebel et al. 2007; Siqueira Mello et al. 2013) and modeling the physical conditions of nucleosynthesis to reproduce this pattern (e.g., Wanajo et al. 2003; Kratz et al. 2007; Qian & Wasserburg 2007; Hayek et al. 2009). Other approaches include estimating the frequency of *r*-II stars in the field (Barklem et al. 2005), estimating the frequency of *r*-II stars exhibiting radial velocity variations that reveal unseen companions (Hansen et al. 2011, 2015b), searching for kinematic properties shared by *r*-process-enhanced stars (Roederer 2009), searching for subtle abundance patterns among the lighter elements in *r*-II stars (Roederer et al. 2014a), probing the extent to which *r*-process material can be detected in trace amounts in metal-poor stars (Roederer 2013; Roederer et al. 2014c), modeling the light curves associated with *r*-process events that might be found in transient surveys (Metzger et al. 2010; Goriely et al. 2011; Kasen et al. 2015), and searching for short-lived radioactive nuclides produced by the *r*-process in deep-sea crust or sediments (Hotokezaka et al. 2015; Wallner et al. 2015). Others pursue this question by modeling the chemical evolution of *r*-process elements integrated across the Galactic halo (e.g., Mathews et al. 1992; Ishimaru & Wanajo 1999; Argast et al. 2004; Matteucci et al. 2014; Cescutti et al. 2015), within dwarf spheroidal (dSph) galaxies (Tsujimoto & Shigeyama 2014), or within cosmologically motivated galaxy merger models and simulations (Komiya et al. 2014; Ishimaru et al. 2015; Shen et al. 2015; van de Voort et al. 2015). The growing preponderance of evidence appears to point toward neutron star mergers as a dominant source of *r*-process material, but definitive observational evidence is still lacking.

Here, we present a detailed abundance analysis of four stars in Ret 2. We confirm the abundances of Fe, Ba, and Eu reported by Ji et al. (2015a), and we expand the chemical inventory to include 20 elements from C ($Z = 6$) to Dy ($Z = 66$). We also present upper limits for six other elements. We present the new observational material in Section 2, outline our analysis in Section 3, describe our results in Section 4, and discuss their implications in Section 5.

2. OBSERVATIONS

There are only four stars brighter than the horizontal branch that are confirmed members of Ret 2 (Simon et al. 2015; Walker et al. 2015). Table 1 lists the g magnitudes and $g - r$ colors, adopted from the photometric catalogs that Koposov et al. (2015a) generated from public DES images. The DES names are listed in Table 1. Throughout this paper, we refer to these stars by the shorter names listed in Table 1.

We observed these four stars using one arm of the Michigan/*Magellan* Fiber System (M2FS) and MSpec double spectrograph (Bailey et al. 2012; Mateo et al. 2012) mounted on the Nasmyth platform at the 6.5 m Landon Clay Telescope (*Magellan* II) at Las Campanas Observatory, Chile. We observed four high-probability members of Ret 2 and one blank sky position simultaneously on 2015 November 14 and 16, with a total integration time of 6.67 hr. Both observations were taken in dark time.

Our observations were made using the HiRes mode of M2FS with 95 μm entrance slits. This setup delivered spectral resolving power $R \equiv \lambda/\Delta\lambda \sim 30{,}000$, as measured from isolated Th or Ar emission lines in the comparison lamp spectra. We use a new custom order-isolation filter to observe orders 66–86, which covers roughly $4150 \leqslant \lambda \leqslant 5430$ Å for each target. Figure 1 illustrates sections of the M2FS spectra of these four stars.

Some data reduction (merging data from different CCD chip amplifiers, stacking images, masking cosmic rays, and subtracting scattered light) was performed using custom routines. Standard IRAF routines were used to perform all other tasks (flatfielding, extraction, wavelength calibration, spectra co-addition, velocity shifting, and continuum normalization). Sky contamination was found to be negligible, so no sky subtraction was performed. Table 1 also lists the signal-to-noise ratios (S/N) per pixel for the co-added spectra at several wavelengths.

3. ANALYSIS

3.1. Radial Velocities

We measure radial velocities using the IRAF *fxcor* task to cross-correlate the order containing the Mg I b lines against a template. We use the highest S/N spectrum in our sample (Star 4, observation 2) as the template. We set the zeropoint of this spectrum by measuring the offset between observed and laboratory wavelengths of several Mg I and Fe I lines. We adopt laboratory wavelengths from the Atomic Spectra Database (ASD) of the National Institute of Standards and Technology (NIST; Kramida et al. 2015). The velocity zeropoint of the template is accurate to $\sim$0.2 km s^{-1}. We reproduce the radial velocities of two standard stars (CD–43°2527 and HD 48381) observed on each night to within 0.5 km s^{-1} rms (Udry et al. 1999). Roederer et al. (2016) reported radial velocity measurement uncertainties $\sim$0.7–1.0 km s^{-1} using the same M2FS entrance slits based on repeat observations of stars with comparable S/N. We estimate that the uncertainties on our radial velocity measurements do not exceed 1.0 km s^{-1}. The two velocity measurements for each star show no evidence of variations.

We report mean heliocentric radial velocities, V_r, for each star in Table 1. We calculate heliocentric corrections using the IRAF *rvcorrect* task. The velocities in Table 1 represent an unweighted mean of our two observations. We find reasonable agreement between our radial velocities and those measured by Koposov et al. (2015b), Simon et al. (2015), and Walker et al. (2015), as reported in Table 2.

Table 1
Basic Stellar Data

Name[a]	Name[b]	Name[c]	g	$g-r$	V_r (km s^{-1})	S/N 4300 Å	S/N 4800 Å	S/N 5200 Å
Star 1	DES J033447.94–540525.0	Ret2–80	17.50	0.59	+62.2	17	26	33
Star 2	DES J033523.85–540407.5	⋯	16.47	0.80	+65.5	15	26	35
Star 3	DES J033531.14–540148.2	Ret2–115	17.57	0.56	+59.7	25	40	48
Star 4	DES J033607.75–540235.6	Ret2–178	17.39	0.58	+62.0	26	45	59

Notes.
[a] This study.
[b] Simon et al. (2015).
[c] Walker et al. (2015).

(This table is available in machine-readable form.)

3.2. Equivalent Widths (EWs) and Atomic Data

We measure EWs from the spectra using a semi-automated routine that fits Voigt (or Gaussian) line profiles to continuum-normalized spectra. As discussed in Roederer et al. (2014b), the user must visually inspect all lines, and poor fits can be modified by hand. Table 3 lists the EWs measured from our data. Roederer et al. (2016) showed that the EWs measured from M2FS HiRes spectra taken with the same 95 μm entrance slits agree to better than 1 mÅ with those derived from MIKE spectra, which were shown by Bedell et al. (2014) and Roederer et al. (2014b) to agree with high-resolution spectra taken at several observatories.

Table 3 also includes the wavelengths (λ), identifications, excitation potentials (EP), and log gf values for all lines. We use log gf values from recent laboratory studies whenever possible, since these investigations frequently deliver ∼5% precision (0.02 dex) or better (e.g., Lawler et al. 2009).

3.3. Stellar Parameters and Abundance Analysis

We base our estimates of the stellar parameters on measures that can be extracted from the spectra themselves. We interpolate model atmospheres from the one-dimensional plane-parallel ATLAS9 grid of α-enhanced models (Castelli & Kurucz 2003). We compute Fe abundances from Fe I and Fe II lines using a recent version of the spectrum analysis code MOOG (Sneden 1973; Sobeck et al. 2011), which assumes local thermodynamic equilibrium for the line-forming layers of the atmosphere.

We derive the effective temperatures ($T_{\rm eff}$), log of the surface gravity (log g), microturbulence ($v_{\rm t}$), and model metallicity ([M/H]) using an iterative process. We start from an initial guess appropriate for typical metal-poor red giant stars, but this initial set of parameters has no substantial impact on the final set. We estimate $T_{\rm eff}$ by requiring no correlation between the EP of Fe I lines and the abundances derived from them. We simultaneously require no correlation between these abundances and the line strength, which sets $v_{\rm t}$. Spectroscopic $T_{\rm eff}$ values like these are known to be systematically cooler by a few percent than those derived from color–$T_{\rm eff}$ relations (e.g., Johnson 2002). Recent measures of the angular diameter of the nearby metal-poor giant HD 122563 by Creevey et al. (2012) favor photometric $T_{\rm eff}$ scales, so we correct our spectroscopic $T_{\rm eff}$ values to a photometric scale using the relation given by Frebel et al. (2013). The uncertainty in $T_{\rm eff}$ is dominated by the scatter in this calibration.

We next calculate log g from the set of Y^2 α-enhanced isochrones (Demarque et al. 2004) using our adjusted $T_{\rm eff}$ as the input. We assume a uniform old age (13 Gyr; cf., e.g., Brown et al. 2012) for all stars. We propagate uncertainties from $T_{\rm eff}$ into log g using 10^4 Monte Carlo calculations. The 13 Gyr [Fe/H] = −2.5 and −3.3 isochrones predict log g different by only 0.06 dex for red giants, and an assumed age of 10 Gyr instead of 13 Gyr only changes the predicted log g by 0.03 dex. These are insignificant compared to the uncertainty introduced by $T_{\rm eff}$.

We then rederive abundances using the new log g value, recalculating the $v_{\rm t}$ value and ignoring the slight correlation between EP and abundance. We also set [M/H] equal to the Fe abundance derived from Fe II lines. (No Fe II lines are measurable in Star 1, so we set [M/H] equal to the abundance derived from Fe I lines.) We iterate these steps until the model converges. Throughout this process we cull lines (∼10% of the lines) whose derived abundance deviates from the mean by more than 2σ. The final model atmosphere parameters and their uncertainties are listed in Table 4. Our $T_{\rm eff}$ and log g values are in excellent agreement with the values derived by Ji et al. (2015a), as shown in Table 2.

We derive most abundances using an adaptation of the batch mode capabilities of MOOG. This method generates theoretical EWs that are forced to match the measured ones by adjusting the abundance of each element. Lines that are blended or broadened by hyperfine splitting (HFS) structure or isotope shifts (IS) are measured by comparing to a set of synthetic spectra generated by MOOG. We adopt r-process isotopic fractions for Ba, Nd, Sm, and Eu (Sneden et al. 2008). We derive C abundances by matching synthetic spectra to the observed CH $A^2\Delta - X^2\Pi$ G band from 4290 to 4330 Å, using a line list provided by B. Plez (2007, private communication). We derive 3σ upper limits based on non-detections using the method described in Roederer et al. (2014b).

4. RESULTS

Table 5 lists the abundances derived from each line in each star. Tables 6 and 7 list the mean abundances and their uncertainties. For element X, the logarithmic abundance is defined as the number of atoms of element X per 10^{12} H atoms, $\log\epsilon({\rm X}) \equiv \log_{10}(N_{\rm X}/N_{\rm H}) + 12.0$. For elements X and Y, the logarithmic abundance ratio relative to the solar ratio is defined as $[{\rm X/Y}] \equiv \log_{10}(N_{\rm X}/N_{\rm Y}) - \log_{10}(N_{\rm X}/N_{\rm Y})_{\odot}$. These ratios are constructed by referencing abundances derived from species in the same ionization state (i.e., neutrals to neutrals and ions to ions). We adopt the solar reference abundances given in Asplund et al. (2009).

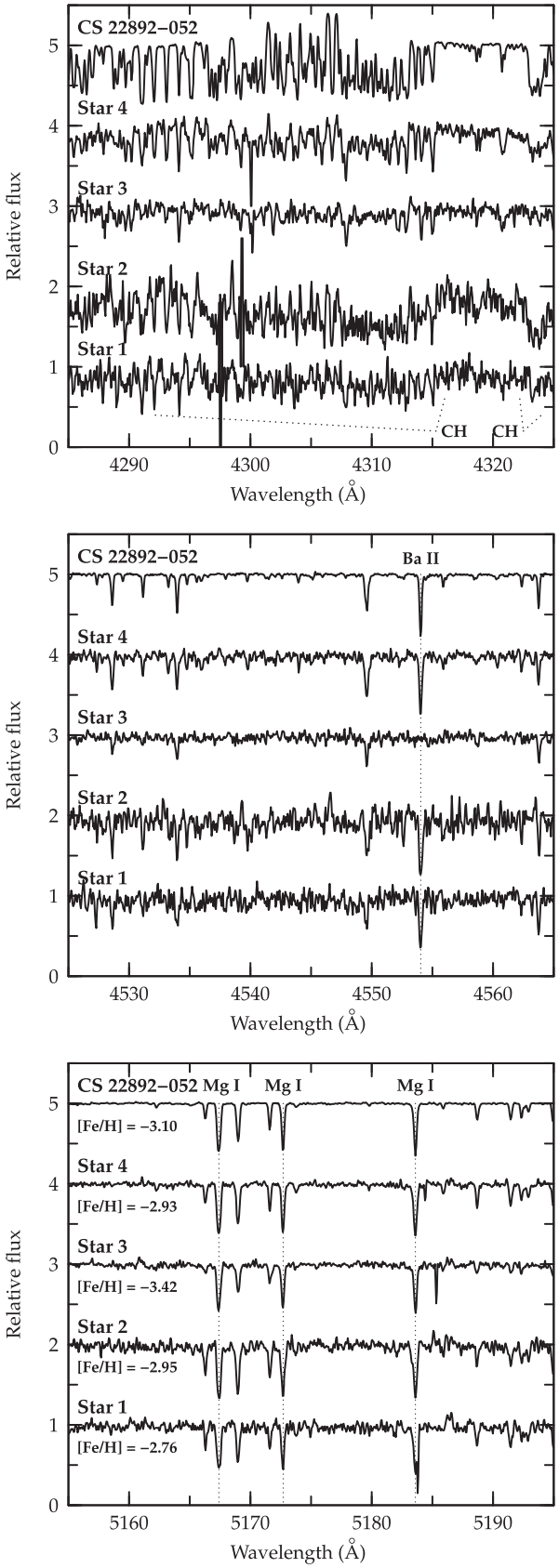

Figure 1. Selections of the normalized M2FS spectra of four stars in Ret 2 and CS 22892–052 around the CH G band (top), Ba II line at 4554 Å (middle), and Mg I b triplet (bottom). The spectra have been offset vertically for display purposes.

Table 2
Comparison with Previous Studies

Quantity	Study	$\langle\Delta\rangle$[a]	σ	N
V_r (km s^{-1})	Simon et al. (2015)	+1.2 ± 0.8	1.6	4
	Walker et al. (2015)	−0.3 ± 0.4	0.7	3
	Koposov et al. (2015b)	−0.3	⋯	2
$T_{\rm eff}$ (K)	Ji et al. (2015a)	+32 ± 47	93	4
log g	Ji et al. (2015a)	+0.07 ± 0.15	0.29	4
[Fe/H]	Simon et al. (2015)	−0.20 ± 0.10	0.18	3
	Walker et al. (2015)	−0.22 ± 0.28	0.48	3
	Koposov et al. (2015b)	−0.68	⋯	2
	Ji et al. (2015a)	+0.04 ± 0.05	0.09	4
[Ba/Fe]	Ji et al. (2015a)	−0.11 ± 0.20	0.35	3
[Eu/Fe]	Ji et al. (2015a)	−0.11 ± 0.07	0.11	3

Note.
[a] Differences in the sense of our study minus previous study.

Four sets of uncertainties are listed in Tables 6 and 7. These are calculated as described in Roederer et al. (2014b), based on the methodology of McWilliam et al. (1995). The statistical uncertainty, $\sigma_{\rm stat}$, is given by Equation (A17) of McWilliam et al. and includes uncertainties in the EW, line profile fitting, and log gf values. The total uncertainty, $\sigma_{\rm tot}$, is given by Equation (A16) of McWilliam et al. and includes the statistical uncertainty and uncertainties in the model atmosphere parameters. We use the other two uncertainties, $\sigma_{\rm I}$ and $\sigma_{\rm II}$, when constructing abundance ratios among different elements. We add $\sigma_{\rm I}$ for element X in quadrature with $\sigma_{\rm stat}$ for element Y when computing the ratio [X/Y] when Y is derived from lines of the neutral species. Similarly, we add $\sigma_{\rm II}$ for element X in quadrature with $\sigma_{\rm stat}$ for element Y when Y is derived from lines of the ionized species.

Our derived metallicities are in reasonable agreement with those derived by Ji et al. (2015a), Simon et al. (2015), and Walker et al. (2015). The mean metallicity difference calculated from two stars in common with Koposov et al. (2015b) is −0.68 dex. Table 2 also lists these comparisons. We are encouraged by the general agreement in light of the different methods, spectral coverage, and S/N that are used to derive [Fe/H]. Table 2 also compares our derived [Ba/Fe] and [Eu/Fe] ratios with those of Ji et al. These values are in good agreement.

4.1. Neutron-capture Elements

Figure 2 compares the [Sr/Fe], [Ba/Fe], and [Eu/Fe] ratios in the Ret 2 stars with those in other UFD galaxies and halo stars in the solar neighborhood. The Sr II line at 4215 Å is detectable (Figure 3) in the most metal-poor star in Ret 2, Star 3, but no other transitions of any n-capture element are detectable in our spectrum of this star. The upper limit derived from the Ba II line at 4554 Å is among the lowest for any stars with [Fe/H] < -3 in the UFD galaxies.

The n-capture abundances observed in the other three stars in Ret 2 are unprecedented among the UFD galaxies. All three show extremely enhanced ratios of [Ba/Fe], [Eu/Fe], and other heavy elements. Figure 3 compares a piece of the spectrum of Star 4 ($T_{\rm eff}$ = 4810 K, [Fe/H] = −2.93, [Eu/Fe] = +1.64) with two other metal-poor red giants. One star is in the UFD galaxy Seg 2 ($T_{\rm eff}$ = 4566 K, [Fe/H] = −2.96, [Eu/Fe] < −0.30; Roederer & Kirby 2014). That study detected a total of

Table 3
Equivalent Widths and Atomic Data

Species	λ (Å)	EP (eV)	log *gf*	Ref.	EW Star 1 (mÅ)	EW Star 2 (mÅ)	EW Star 3 (mÅ)	EW Star 4 (mÅ)
Mg I	4571.10	0.00	−5.62	1	45.2	90.8	53.0	39.2
Mg I	4702.99	4.33	−0.38	1	63.9	55.7	59.5	71.1

Note. The word "synth" in the EW columns indicates that abundances were derived by spectral synthesis matching. The word "limit" indicates that a 3σ upper limit was derived from a non-detection.

References. (1) Kramida et al. (2015), (2) Aldenius et al. (2007), (3) Lawler & Dakin (1989), using HFS from Kurucz & Bell (1995), (4) Lawler et al. (2013), (5) Wood et al. (2013), (6) Lawler et al. (2014), (7) Sobeck et al. (2007), (8) Nilsson et al. (2006), (9) Booth et al. (1984), (10) Den Hartog et al. (2011) for both log *gf* value and HFS; (11) Ruffoni et al. (2014), (12) Wood et al. (2014), (13) Kramida et al. (2015), using HFS from Kurucz & Bell (1995), (14) Roederer & Lawler (2012), (15) Biémont et al. (2011), (16) Ljung et al. (2006), (17) Palmeri et al. (2005), (18) Wickliffe et al. (1994), (19) Kramida et al. (2015), using HFS/IS from McWilliam (1998) when available, (20) Lawler et al. (2001a), using HFS from Ivans et al. (2006), (21) Lawler et al. (2009), (22) Li et al. (2007), using HFS from Sneden et al. (2009), (23) Ivarsson et al. (2001), using HFS from Sneden et al. (2009), (24) Den Hartog et al. (2003), using HFS/IS from Roederer et al. (2008a) when available, (25) Lawler et al. (2006), using HFS/IS from Roederer et al. (2008a) when available, (26) Lawler et al. (2001c), using HFS/IS from Ivans et al. (2006), (27) Den Hartog et al. (2006), (28) Lawler et al. (2001b), using HFS from Lawler et al. (2001d) when available, (29) Wickliffe et al. (2000).

(This table is available in its entirety in machine-readable form.)

Table 4
Stellar Parameters

Name	$T_{\rm eff}$ (K)	log *g*	$v_{\rm t}$ (km s^{-1})	[*M*/*H*]
Star 1	5020 (140)	2.09 (0.38)	2.00 (0.3)	−2.7 (0.2)
Star 2	4710 (140)	1.22 (0.40)	2.85 (0.3)	−2.9 (0.2)
Star 3	4855 (140)	1.63 (0.39)	2.40 (0.2)	−3.3 (0.2)
Star 4	4810 (140)	1.50 (0.39)	2.15 (0.2)	−2.8 (0.2)

(This table is available in machine-readable form.)

Table 5
Abundances Derived from Individual Lines

Star	Species	λ (Å)	log ϵ	σlog ϵ
Star 1	Mg I	4571.10	+5.28	0.20
Star 1	Mg I	4702.99	+5.14	0.26

(This table is available in its entirety in machine-readable form.)

seven lines of *n*-capture elements in the star in Seg 2: 2 lines of Sr II and 5 lines of Ba II. In contrast, numerous lines of *n*-capture elements are detectable in Star 4 in Ret 2. The spectrum of this star closely resembles that of the metal-poor *r*-process-enhanced field giant CS 22892–052 ($T_{\rm eff}$ = 4800 K, [Fe/H] = −3.10, [Eu/Fe] = +1.64; Sneden et al. 2003). The only substantial differences between the spectra of Star 4 and CS 22892–052 are the CH features, since CS 22892–052 is C-enhanced ([C/Fe] = +0.88, Sneden et al.). These three stars in Ret 2 have a mean metallicity ([Fe/H] = −2.88 ± 0.10) in the same range as most *r*-II stars found in the halo, roughly $-3.2 \lesssim$ [Fe/H] $\lesssim -2.6$ (e.g., Barklem et al. 2005; Roederer et al. 2014a).

Figure 4 illustrates the detailed abundance patterns of each of the four stars observed in Ret 2. The abundance pattern found in star CS 22892–052 is shown for comparison. The only adjustment made to this pattern is its overall normalization. This pattern is a superb representation for the elements detected in Star 1, Star 2, and Star 4 in Ret 2. The ratio between the lighter *n*-capture elements (Sr, Y, and Zr; $38 \leqslant Z \leqslant 40$) and the heavier ones (Ba and beyond; $Z \geqslant 56$) is also well-matched, which is not always the case in metal-poor stars with *r*-process material (e.g., McWilliam 1998; Johnson & Bolte 2002; Aoki et al. 2005; Roederer et al. 2010). This comparison also suggests that the radioactive actinides ^{232}Th and ^{238}U may be present and detectable in Ret 2, which could offer an independent check of the age of the *r*-process material in this system (cf., e.g., Cowan et al. 1997; Cayrel et al. 2001), but no lines of these elements are covered in our spectra. We conclude that *r*-process nucleosynthesis is responsible for the production of the heavy elements observed in Ret 2.

4.2. Carbon

The [C/Fe] ratios in all four stars observed in Ret 2 are super-solar, as shown in Figure 2. However, C is depleted at the surface as stars ascend the red giant branch. We use the corrections given by Placco et al. (2014) to estimate the natal [C/Fe] ratios for these stars. These are listed in Table 8. The magnitude of the corrections increases with decreasing log *g*, as expected. Star 2 is classified as a C-enhanced metal-poor (CEMP) star using a common definition of C-enhancement, [C/Fe] > +0.7 (Aoki et al. 2007a). The enhanced C in Star 2 is apparent from the strong absorption near 4310 and 4323 Å in the top panel of Figure 1.

The fraction of CEMP stars in the field increases with decreasing metallicity (e.g., Frebel et al. 2006; Carollo et al. 2012; Lee et al. 2013b; Placco et al. 2014). CEMP stars with no enhancement of slow *n*-capture process (*s*-process) material, like those in Ret 2, likely reflect their natal composition (e.g., Ryan et al. 2005; Norris et al. 2013; Starkenburg et al. 2014; Hansen et al. 2015a, 2015c). These CEMP stars may contain metals from one or a few zero-metallicity Pop III stars (cf., e.g., Bromm & Loeb 2003; Umeda & Nomoto 2005; Cooke & Madau 2014; Ishigaki et al. 2014b), although they are not the only class of stars proposed to have formed from the remnants of Pop III stars (e.g., Aoki et al. 2014). A few CEMP stars have been identified in the UFD galaxies (Frebel et al. 2010; Norris et al. 2010a; Lai et al. 2011; Gilmore et al. 2013), and we add one star in Ret 2 to this small but growing inventory.

The CEMP star in Ret 2 is also substantially enhanced in *r*-process material (CEMP-*r*, according to the nomenclature of Beers & Christlieb 2005). Only two other stars, CS 22892–052 (Sneden et al. 1994, 1996) and CS 22945–017 (Roederer et al.

Table 6
Mean Abundances I

	Star 1							Star 2						
Species	N	log ϵ	[X/Fe][a]	σ_{stat}	σ_{tot}	σ_{I}	σ_{II}	N	log ϵ	[X/Fe][a]	σ_{stat}	σ_{tot}	σ_{I}	σ_{II}
Fe I	21	+4.74	−2.76	0.09	0.19	0.00	0.00	30	+4.55	−2.95	0.11	0.21	0.00	0.00
Fe II	0	...	...	...	...	...	...	4	+4.55	−2.95	0.14	0.20	0.00	0.00
C (CH)	1	+5.92	+0.25	0.25	0.31	0.31	0.31	1	+6.08	+0.60	0.25	0.32	0.32	0.32
Mg I	3	+5.17	+0.33	0.08	0.20	0.12	0.12	4	+5.03	+0.38	0.09	0.24	0.15	0.24
Ca I	0	...	...	...	...	...	...	0	...	...	...	...	...	...
Sc II	0	...	...	...	...	...	...	1	<+0.55	<+0.35	0.21	0.26	0.31	0.26
Ti I	4	+2.85	+0.66	0.08	0.19	0.12	0.12	4	+2.57	+0.56	0.11	0.21	0.15	0.25
Ti II	3	+2.31	+0.12	0.11	0.19	0.22	0.12	3	+2.38	+0.39	0.10	0.17	0.23	0.17
V I	0	...	...	...	...	...	...	0	...	...	...	...	...	...
Cr I	2	+2.64	−0.23	0.10	0.19	0.13	0.13	3	<+2.96	<+0.27	...	...	...	...
Cr II	0	...	...	...	...	...	...	0	...	...	...	...	...	...
Mn I	0	...	...	...	...	...	...	0	...	...	...	...	...	...
Ni I	0	...	...	...	...	...	...	1	<+4.57	<+1.30	...	...	...	...
Zn I	0	...	...	...	...	...	...	0	...	...	...	...	...	...
Sr II	1	+0.70	+0.59	0.48	0.51	0.51	0.47	1	+0.46	+0.54	0.23	0.26	0.27	0.30
Y II	3	−0.13	+0.42	0.16	0.21	0.26	0.17	5	−0.34	+0.41	0.19	0.24	0.29	0.23
Zr II	1	+0.69	+0.87	0.37	0.40	0.42	0.38	2	<+0.65	<+1.02	...	...	...	...
Tc I	0	...	...	...	...	...	...	0	...	...	...	...	...	...
Ru I	1	<+2.35	<+3.36	...	...	...	...	1	<+1.93	<+3.13	...	...	...	...
Ba II	1	+0.22	+0.80	0.17	0.24	0.25	0.17	1	+0.32	+1.09	0.21	0.24	0.25	0.28
La II	1	−0.24	+1.42	0.17	0.22	0.26	0.18	2	−0.49	+1.36	0.20	0.25	0.30	0.25
Ce II	1	+0.09	+1.27	0.12	0.19	0.24	0.14	5	−0.11	+1.26	0.19	0.24	0.29	0.23
Pr II	1	−0.27	+1.77	0.41	0.43	0.46	0.41	2	−0.66	+1.57	0.26	0.30	0.35	0.30
Nd II	6	+0.35	+1.69	0.14	0.19	0.24	0.15	7	−0.07	+1.46	0.17	0.23	0.28	0.22
Sm II	2	+0.11	+1.91	0.15	0.20	0.25	0.16	3	−0.17	+1.82	0.18	0.24	0.28	0.23
Eu II	2	−0.49	+1.75	0.27	0.32	0.33	0.27	2	−0.75	+1.68	0.14	0.18	0.23	0.20
Gd II	2	<+0.64	<+2.33	...	...	...	...	2	<+0.37	<+2.25	...	...	...	...
Tb II	0	...	...	...	...	...	...	1	<−0.78	<+1.87	...	...	...	...
Dy II	1	<+0.52	<+2.18	...	...	...	...	1	+0.09	+1.94	0.32	0.40	0.40	0.39

Note.
[a] [Fe/H] given for Fe I and Fe II.

2014a) are members of the CEMP-*r* class. No compelling explanation exists for the enhancement of both C and *r*-process material in these stars. Not all *r*-process stars in Ret 2 are C-enhanced. We infer from this that the C and *r*-process enhancements may not be co-produced by the same nucleosynthesis site or mechanism. By extension, perhaps the C- and *r*-process-enhancements in other CEMP-*r* stars are also not directly related, as previous studies have concluded.

4.3. Magnesium through Zinc

Figure 2 also compares the abundance ratios among α- and Fe-group elements in Ret 2 with those in other UFD galaxies and halo giants. In all cases, the Ret 2 abundance ratios fall well within the range found for other UFD galaxies and halo stars.

The [Mg/Fe] ratio is higher in Star 3, the most metal-poor star in Ret 2 observed by us, by ≈0.45 dex compared to the other three stars. This difference is about three times larger than the measurement uncertainties. Figure 5 illustrates portions of the spectra around several Mg I lines in Star 3 and Star 4, which have different [Fe/H] but similar [Mg/H] ratios. This comparison supports our assertion that the [Mg/Fe] ratio is enhanced in Star 3. Enhanced [Mg/Fe] appears to be a genuine characteristic of some stars in the UFD galaxies. Two of these Mg-enhanced stars (in Boo I and Seg 1) are also C-enhanced (Norris et al. 2010a; Lai et al. 2011; Gilmore et al. 2013), but the one in Ret 2 and several others in Com, Her, and UMa II are not (Koch et al. 2008; Frebel et al. 2010). The enhanced [Mg/Fe] ratios in the C-normal stars have been interpreted (e.g., Koch et al.) as evidence for enrichment dominated by high-mass core-collapse supernovae.

[Ti I/Fe] is high in three of the four stars. The Ti I abundance has been derived from 4–12 lines in these three stars. No line appears to yield systematically high abundances in Ret 2, and Roederer et al. (2014b) did not identify any of these lines as yielding systematically high abundances in metal-poor halo giants. This indicates that the high [Ti I/Fe] ratios cannot be attributed to a handful of blended or poorly measured Ti I lines. We note that [Ti II/Fe] is not high, however, suggesting that there is probably not a genuine excess of Ti in the Ret 2 stars.

The [X/Fe] ratios show minimal or no dispersion within Ret 2, except for C, Mg, and the *n*-capture elements discussed previously. Furthermore, none of the [Mg/Fe], [Ca/Fe], or [Ti/Fe] ratios lie significantly below the α-enhanced plateau ([α/Fe] ∼ +0.3) in any of the Ret 2 stars observed.

4.4. Outliers in the [X/Fe] Ratios

In Figure 6, we perform a detailed quantitative comparison between the abundance ratios in each of the stars in Ret 2 and halo giants with similar T_{eff} and [Fe/H] that have been analyzed using similar methods. This comparison allows us to identify any element ratios that are outliers relative to the majority of halo stars. The systematic abundance uncertainties largely cancel out when using this differential approach. Elements detected in multiple ionization states are compared and

Table 7
Mean Abundances II

	Star 3							Star 4						
Species	N	log ϵ	[X/Fe][a]	σ_{stat}	σ_{tot}	σ_{I}	σ_{II}	N	log ϵ	[X/Fe][a]	σ_{stat}	σ_{tot}	σ_{I}	σ_{II}
Fe I	28	+4.08	−3.42	0.11	0.20	0.00	0.00	51	+4.57	−2.93	0.06	0.18	0.00	0.00
Fe II	2	+4.24	−3.26	0.10	0.17	0.00	0.00	6	+4.71	−2.79	0.07	0.15	0.00	0.00
C (CH)	1	+5.14	+0.13	0.15	0.25	0.19	0.19	1	+5.76	+0.26	0.15	0.25	0.19	0.19
Mg I	4	+4.99	+0.81	0.08	0.21	0.14	0.23	4	+5.01	+0.34	0.05	0.19	0.09	0.20
Ca I	1	+3.08	+0.16	0.28	0.32	0.30	0.34	2	+3.76	+0.36	0.13	0.21	0.14	0.23
Sc II	1	<+0.79	<+0.90	…	…	…	…	1	<+0.70	<+0.34	…	…	…	…
Ti I	3	+1.88	+0.35	0.13	0.21	0.17	0.24	12	+2.51	+0.50	0.05	0.17	0.08	0.20
Ti II	4	+1.94	+0.25	0.14	0.19	0.24	0.18	9	+2.55	+0.39	0.06	0.15	0.20	0.09
V I	6	<+1.21	<+0.70	…	…	…	…	6	<+1.24	<+0.24	…	…	…	…
Cr I	1	<+2.23	<+0.01	…	…	…	…	5	+2.49	−0.22	0.06	0.18	0.08	0.20
Cr II	1	<+3.35	<+0.97	…	…	…	…	3	+3.50	+0.65	0.06	0.15	0.20	0.09
Mn I	0	…	…	…	…	…	…	2	<+2.38	<−0.12	…	…	…	…
Ni I	1	<+3.95	<+1.15	…	…	…	…	1	+3.50	+0.21	0.09	0.19	0.11	0.21
Zn I	3	<+2.14	<+1.00	…	…	…	…	1	+1.96	+0.33	0.13	0.21	0.14	0.23
Sr II	1	−2.12	−1.73	0.42	0.44	0.47	0.43	1	+0.24	+0.16	0.25	0.29	0.29	0.30
Y II	9	<−1.00	<+0.05	…	…	…	…	7	−0.29	+0.29	0.08	0.16	0.21	0.11
Zr II	2	<+1.22	<+1.90	…	…	…	…	3	+0.36	+0.57	0.19	0.23	0.26	0.21
Tc I	1	<+0.56	<+3.98	…	…	…	…	1	<+0.73	<+3.66	…	…	…	…
Ru I	1	<+1.81	<+3.48	…	…	…	…	1	<+1.77	<+2.95	…	…	…	…
Ba II	1	<−2.59	<−1.51	…	…	…	…	1	+0.06	+0.67	0.09	0.16	0.17	0.18
La II	8	<−1.08	<+1.08	…	…	…	…	5	−0.44	+1.26	0.14	0.20	0.24	0.16
Ce II	6	<−0.21	<+1.47	…	…	…	…	5	−0.13	+1.08	0.09	0.17	0.21	0.11
Pr II	4	<−0.97	<+1.57	…	…	…	…	3	−0.71	+1.36	0.16	0.21	0.25	0.17
Nd II	16	<−0.56	<+1.28	…	…	…	…	18	−0.07	+1.30	0.09	0.16	0.21	0.11
Sm II	10	<−1.04	<+1.26	…	…	…	…	14	−0.27	+1.56	0.09	0.17	0.21	0.11
Eu II	1	<−1.66	<+1.08	…	…	…	…	2	−0.63	+1.64	0.06	0.13	0.14	0.14
Gd II	3	<−0.56	<+1.63	…	…	…	…	1	−0.26	+1.46	0.18	0.23	0.27	0.20
Tb II	1	<−0.52	<+2.44	…	…	…	…	0	<−0.39	<+2.10	…	…	…	…
Dy II	1	<−0.24	<+1.92	…	…	…	…	1	+0.19	+1.88	0.12	0.20	0.22	0.18

Note.
[a] [Fe/H] given for Fe I and Fe II.

illustrated separately in Figure 6. We exclude from the comparison sample any stars that exhibit high levels of *s*-process enrichment, since this characteristic frequently signals that the present-day surface composition of the star has been polluted by a companion and probably does not reflect the natal composition.

The heaviest elements are, of course, significantly over-abundant in Star 1, Star 2, and Star 4 relative to the comparison sample. In Star 3, the Sr and Ba abundances are not only deficient relative to the other stars in Ret 2, but they are also deficient relative to the comparison halo sample. This deficiency is, however, quite normal for stars in the UFD galaxies. Frebel et al. (2014) suggested that this may be a result of a single *n*-capture enrichment event within each galaxy. We can detect only Sr in Star 3, limiting our ability to reliably identify the nucleosynthetic process that produced the heaviest elements in Star 3. Candidates include the weak component of the *r*-process (e.g., Truran et al. 2002; Arcones & Thielemann 2013) and charged particle reactions (e.g., Woosley & Hoffman 1992) operating in core-collapse supernovae or the weak component of the *s*-process (e.g., Raiteri et al. 1991; Pignatari et al. 2008) operating in massive, rapidly rotating stars. The upper limit on Ba in Star 3 (Figure 4) is nearly able to exclude the possibility that the *r*-process pattern found in the *r*-process-enhanced stars is also present in Star 3 at an abundance three orders of magnitude lower. Higher quality spectra of this star could settle the issue. Regardless, it seems likely that at least two *n*-capture enrichment events occurred in Ret 2, which distinguishes it from other UFD galaxies.

None of the other [X/Fe] ratios in Figure 6 differ by more than 2σ between the Ret 2 stars and the comparison sample. We conclude that the α and Fe-group elements studied in Ret 2 were produced in similar proportions by the progenitors responsible for enriching Ret 2 and the stars in the halo comparison sample.

Roederer et al. (2014b) performed this comparison for stars in the *r*-II class. That study concluded that the abundances of elements from Mg to Zn in the *r*-II stars are indistinguishable from those in stars with normal levels of *r*-process material at the limit of the data, about 3.5% (0.015 dex). This result was interpreted to mean that the nucleosynthetic sites responsible for the large *r*-process enhancements in the *r*-II stars did not produce any α- or Fe-group element abundance signatures distinct from normal core-collapse supernovae. Alternatively, the *r*-process nucleosynthetic site(s) produced no α or Fe-group elements at all. We propose that this conclusion also applies to the stars examined in Ret 2.

5. DISCUSSION AND CONCLUSIONS

The present-day stellar mass of Ret 2 ($\sim 2.6 \times 10^3\,M_\odot$; Bechtol et al. 2015) is roughly two orders of magnitude less than the minimum mass necessary to fully sample a standard IMF. Assuming that Ret 2 still retains a substantial fraction of its stars, we would expect to observe the effects of

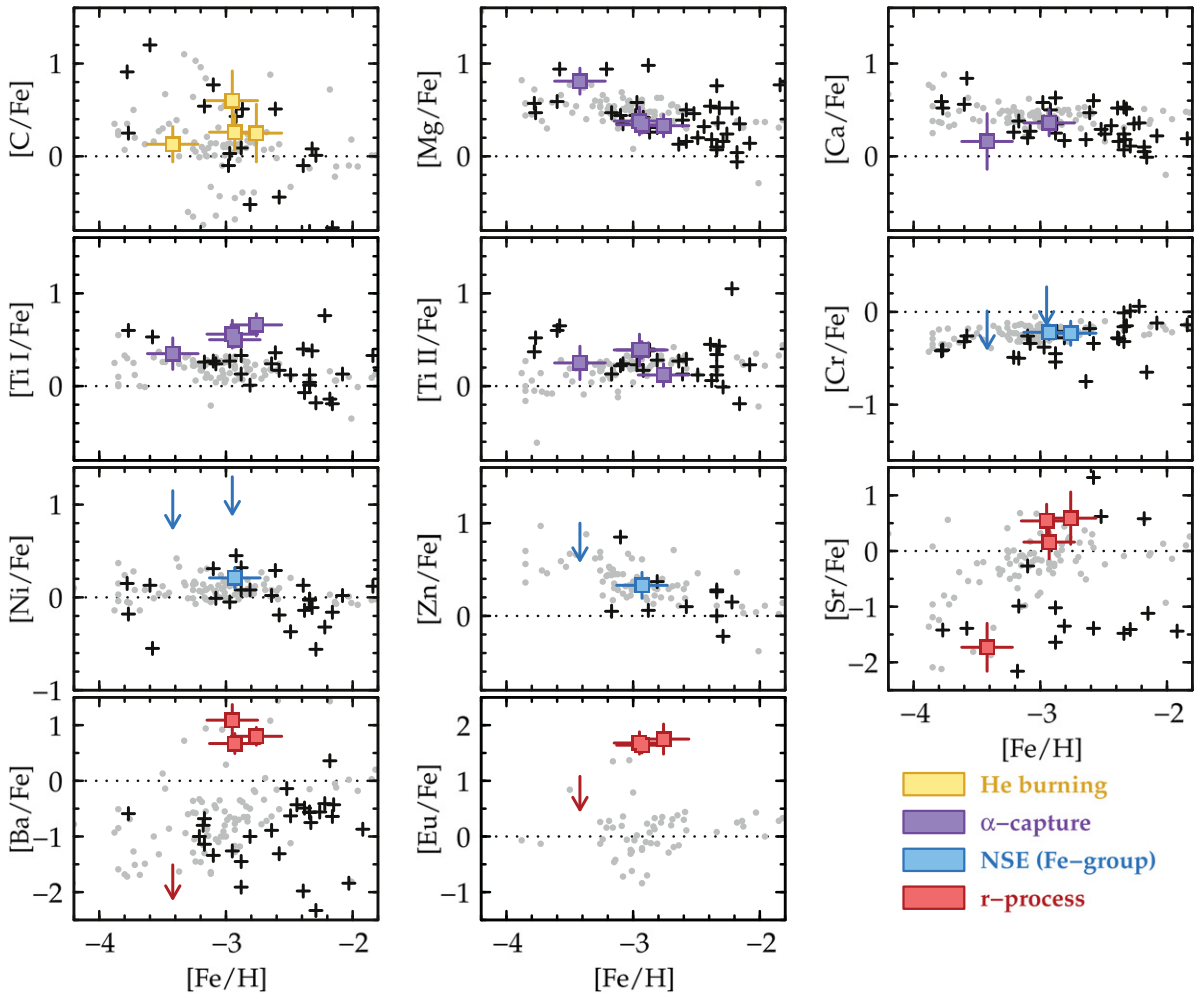

Figure 2. Comparison of abundance ratios in Ret 2 (colored points) with stars in other UFD galaxies (black crosses) and halo giants (gray dots). The UFD sample includes data from Boo I (Feltzing et al. 2009; Norris et al. 2010b; Gilmore et al. 2013; Ishigaki et al. 2014a), Boo II (Koch & Rich 2014; Ji et al. 2015b), CVn II (François et al. 2015), Com (Frebel et al. 2010), Her (Koch et al. 2008, 2013; François et al. 2015), Leo IV (Simon et al. 2010), Seg 1 (Norris et al. 2010a; Frebel et al. 2014), Seg 2 (Roederer & Kirby 2014), and UMa II (Frebel et al. 2010). The halo sample includes only the giants from Roederer et al. (2014b). Upper limits are omitted from the comparison samples for clarity. The colors of the Ret 2 data points indicate the dominant nucleosynthetic origins of each element: yellow, He-burning; green, C and O burning and α-capture in hydrostatic or explosive nucleosynthesis; blue, Fe-group elements formed in nuclear statistical equilibrium (NSE) during explosive nucleosynthesis; red, *r*-process nucleosynthesis. The dotted lines mark the solar ratios. Note the expanded scale on the vertical axes for the [Sr/Fe], [Ba/Fe], and [Eu/Fe] panels.

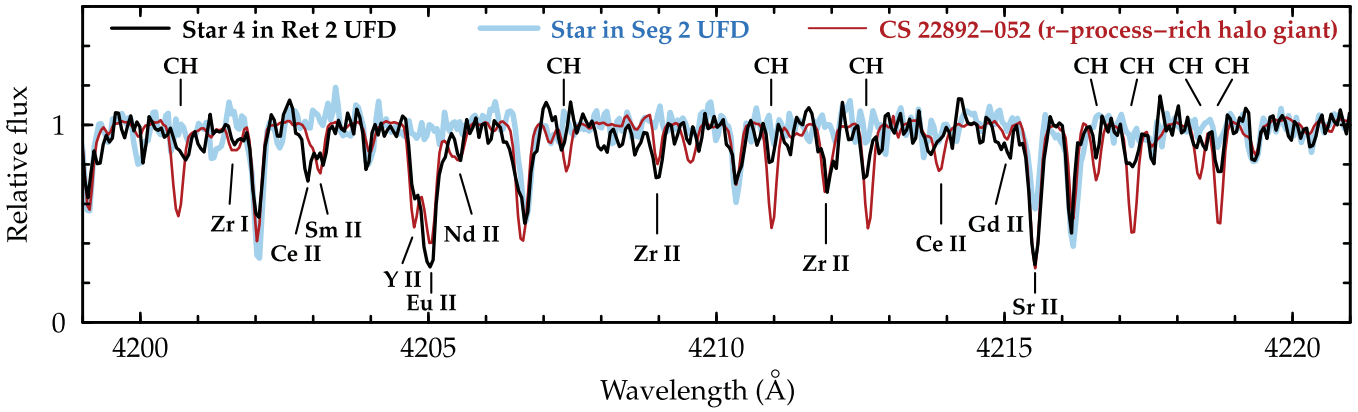

Figure 3. Spectra of Star 4 in Ret 2 (black line), star SDSS J021933.13+200830.2 in Seg 2 (bold blue line), and the field giant CS 22892–052 (thin red line). The SDSS J021933.13+200830.2 and CS 22892–052 spectra were taken using the $R \sim 41{,}000$ setting of the *Magellan* Inamori Kyocera Echelle (MIKE) spectrograph (see Roederer & Kirby 2014 and Roederer et al. 2014b for details). All stars have similar parameters and metallicities, but their C and *n*-capture abundances differ dramatically. Lines of *n*-capture species are marked below the spectra, lines of CH are marked above, and unmarked lines arise from α- or Fe-group elements.

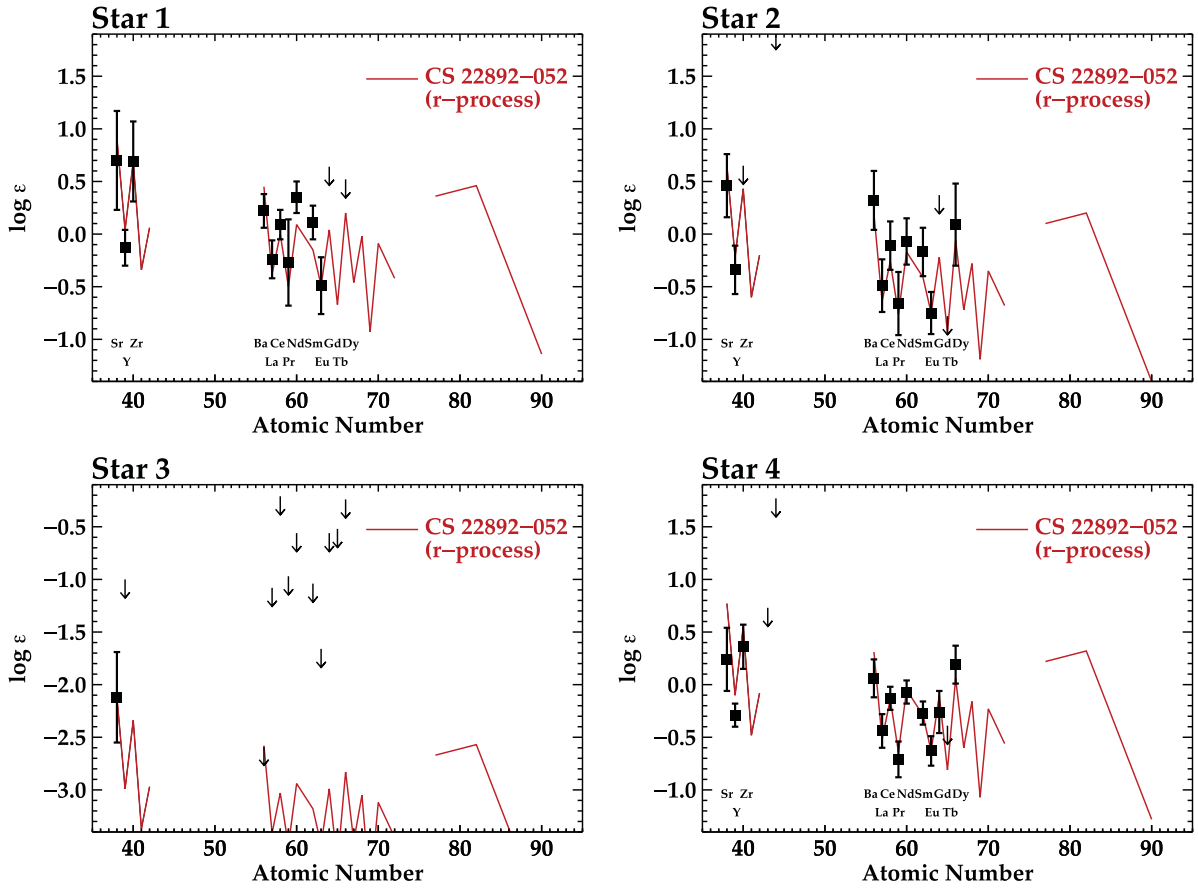

Figure 4. The *n*-capture abundance patterns compared with the *r*-process-enhanced standard star CS 22892–052 (Sneden et al. 2003, 2009; Roederer et al. 2009). The patterns are normalized to Eu ($Z = 63$) in Star 1, Star 2, and Star 4 and to Sr ($Z = 38$) in Star 3. Note the different scale on the vertical axis for Star 3 (lower left panel).

Table 8
Corrected [C/Fe] Ratios

Star	log *g*	[C/Fe] (observed)	[C/Fe] (corrected)
Star 1	2.09	+0.25	+0.27
Star 2	1.22	+0.60	+1.15
Star 3	1.63	+0.13	+0.38
Star 4	1.50	+0.26	+0.68

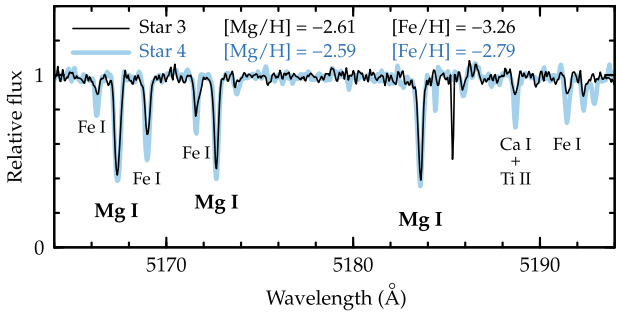

Figure 5. Spectra of Stars 3 and 4 around the Mg I lines at 5167.32, 5172.68, and 5183.60 Å. Both stars have similar $T_{\rm eff}$ and log *g*. The Fe I lines are significantly weaker in Star 3, yet the Mg I lines have nearly equal strengths.

stochastically sampling the IMF. This evidence may be found in the enhanced [C/Fe] ratio in Star 2 and enhanced [Mg/Fe] ratio in Star 3. The normal α- and Fe-group abundances found in most stars offer no compelling evidence of substantial variations at the high end of the IMF in Ret 2.

The UFD enrichment models of Lee et al. (2013a) rely on stochastic sampling of the mass function of supernovae whose *n*-capture yields are more strongly mass-dependent than yields of lighter elements like Ti. These models predict that some *n*-capture-rich stars should be found in the UFDs, and the *r*-process-enhanced stars in Ret 2 confirm this prediction. Neutron-star mergers (e.g., Goriely et al. 2011; Ramirez-Ruiz et al. 2015) or rare *r*-process events associated with core-collapse supernovae, like magnetically induced jets from the proto neutron star (e.g., Fujimoto et al. 2008; Nishimura et al. 2015), can produce a few $10^{-2}\,M_{\odot}$ of *r*-process material and a few $10^{-5}\,M_{\odot}$ of Eu. These are compatible with the observations of Ret 2, and the sites associated with supernovae fulfill the requirement of the Lee et al. model.

We can use Ret 2 and other UFDs to estimate the amount of material produced by the main component of the *r*-process per unit of gas turned into stars. The 10 UFD galaxies whose stars have been observed at high spectral resolution (see references in caption to Figure 2) have a combined stellar mass of $\sim 1.1 \times 10^{5}\,M_{\odot}$ (McConnachie 2012; Bechtol et al. 2015). Ji et al. (2015a) estimated that $\sim 3 \times 10^{-5}\,M_{\odot}$ of Eu ($\sim 3 \times 10^{-2}\,M_{\odot}$ of *r*-process material) are required to match the observations of Ret 2. Thus $\sim 3 \times 10^{-10}\,M_{\odot}$ of Eu ($\sim 3 \times 10^{-7}\,M_{\odot}$ of *r*-process material) is produced per $M_{\odot}$ of gas turned into stars in the 10 UFD galaxies.

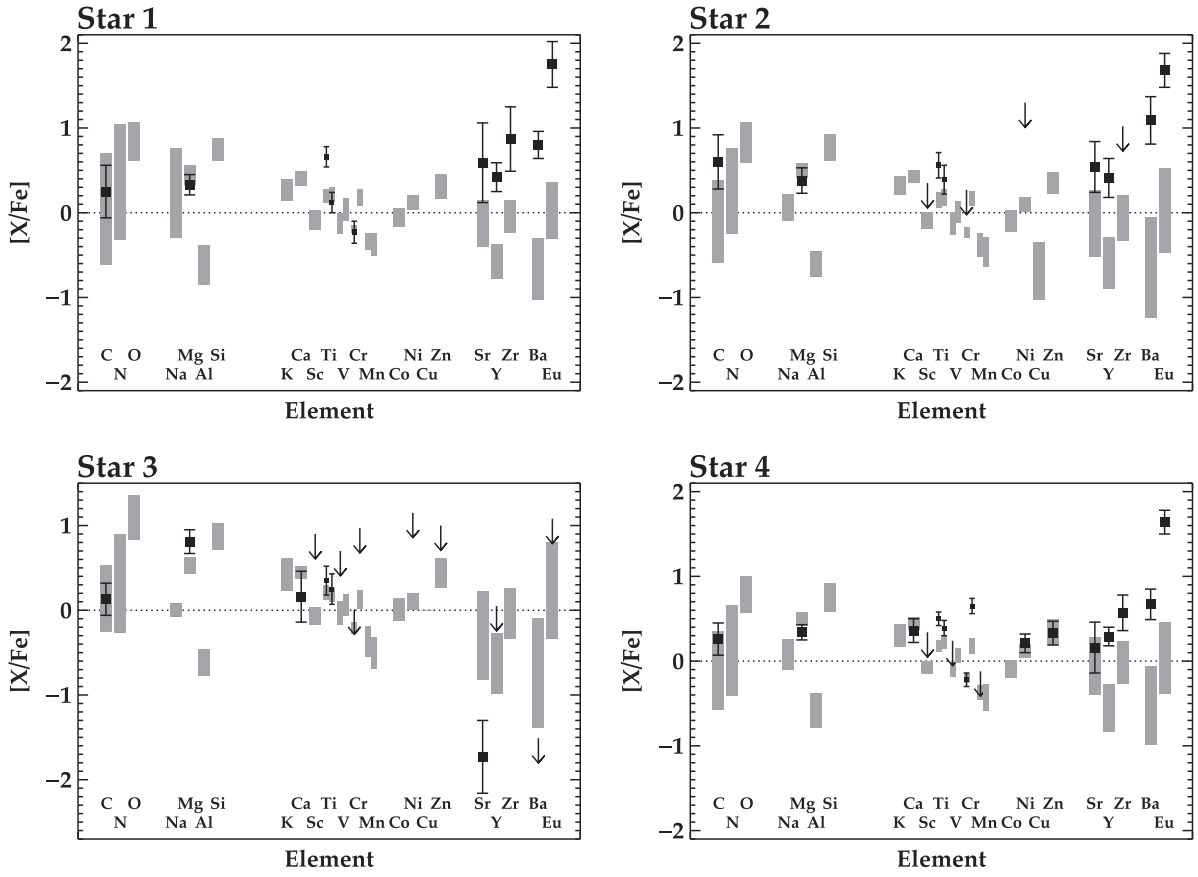

Figure 6. Comparison of the abundances in the Ret 2 stars with field red giants with similar metallicities. The comparison samples, drawn from Roederer et al. (2014b), are selected to have $T_{\rm eff}$ within 250 K and [Fe/H] within 0.3 dex of each Ret 2 star. The number of stars in the comparison samples range from 22 to 34. This comparison sample, shown by the shaded gray boxes, represents the mean $\pm 1\sigma$ standard deviations. Smaller symbols are shown for Ti, V, Cr, and Mn to accommodate ratios from both the neutral and ionized states, which may differ. The dotted line marks the solar ratios.

This rate may offer a link between the UFDs and higher-mass dSph galaxies. Tsujimoto et al. (2015) identified a plateau at [Eu/H] $= -1.3$ in stars with [Fe/H] $\gtrsim -2$ in Dra and several other dSph galaxies. Dra has a total stellar mass of $\sim 2.5 \times 10^5\ M_\odot$ in its stars with [Fe/H] > -2 (Tsujimoto et al.), which translates to $\sim 5 \times 10^{-5}\ M_\odot$ of Eu. Using the rate of Eu production we estimate based on the UFD galaxies, the same stellar mass in Dra would be expected to produce $\sim 7 \times 10^{-5}\ M_\odot$ of Eu. The similarity between these two values could reflect a natural connection between the *r*-process material observed in surviving UFDs and dSph galaxies. Material produced by the main component of the *r*-process has also been found in Car and UMi, two other dSph galaxies with stellar masses similar to Dra (Shetrone et al. 2001, 2003; Sadakane et al. 2004; Cohen & Huang 2010; Venn et al. 2012). The extreme *r*-process enhancement observed in Ret 2 may be the result of a low-probability nucleosynthesis event that becomes inevitable (and less conspicuous) in more luminous dSph galaxies with stellar masses $\gtrsim 10^5\ M_\odot$. Tafelmeyer et al. (2010) and Jablonka et al. (2015) called for examination of the neutron-capture abundance patterns in metal-poor stars in dSph galaxies with a range of masses to better understand the galactic metal retention and (Pop II or Pop III) sites that produce heavy elements. We propose that a focused effort to quantify the fraction of metal-poor stars with material produced by the main component of the *r*-process as a function of galaxy mass may also prove enlightening.

Frebel & Bromm (2012) identified a set of chemical characteristics that could distinguish a bona fide "first galaxy," a system where only one long-lived stellar generation formed from the yields of the first Pop III stars. Ret 2 fulfills some of the observational criteria identified by Frebel & Bromm, since there is no evidence of enrichment by Type Ia supernovae or asymptotic giant branch stars. However, Ret 2 appears not to be a good candidate "first galaxy" based on the large internal spread in *r*-process material. The larger sample of Ji et al. (2015a) hints that chemical evolution may have occurred within Ret 2, since the most metal-poor stars lack the *r*-process enhancements observed in the more metal-rich ones.

The escape velocities of the UFD systems like Ret 2 are $\sim$25–50 km s^{-1}, assuming a NFW halo profile (Navarro et al. 1996) with virial mass $\sim 10^8$–$10^9\ M_\odot$ and a concentration, *c*, of 10.7–12.5 (Prada et al. 2012). Most ($\gg$99%) of the metals produced within Ret 2 were probably lost from the system, as has been inferred for other dwarf galaxies (e.g., Kirby et al. 2011; Frebel et al. 2014). Alternatively, simulations by Smith et al. (2015) indicate that some low-mass minihalos could have been externally enriched by metals from neighboring minihalos prior to formation of their own Pop III star. The star-to-star abundance spreads observed in some element ratios (e.g., [Fe/H], [C/Fe], [Mg/Fe], [Eu/Fe]) indicate that the ISM of Ret 2 was not fully mixed at the time the low-mass stars formed. This indicates that ejecta from at least two supernovae —perhaps even from multiple neighboring minihalos—formed stars in the minihalo that evolved into Ret 2. Simulations

tailored specifically to reproduce the conditions and chemistry in Ret 2 (cf., e.g., Ritter et al. 2015; Webster et al. 2016) may prove illuminating on these points.

We express our deep appreciation to the referee for offering a positive, constructive, and timely review. I.U.R. acknowledges partial support from grant PHY 14-30152 (Physics Frontier Center/JINA-CEE) awarded by the U.S. National Science Foundation (NSF). M.M. and J.I.B. gratefully acknowledge support from NSF grant AST 09-23160 to develop M2FS. S.R.L. acknowledges the Michigan Society of Fellows for financial support. D.L.N. was supported by a McLaughlin Fellowship at the University of Michigan. E.O. is partially supported by NSF grant AST 13-13006. M.V. is supported in part by HST-AR-13890.001, NSF grant AST-09-08346, and NASA-ATP award NNX15AK79G. M.G.W. is supported by NFS grants AST 13-13045 and AST 14-12999. This research has made use of NASA's Astrophysics Data System Bibliographic Services; the arXiv pre-print server operated by Cornell University; the SIMBAD database hosted by the Strasbourg Astronomical Data Center; the ASD hosted by NIST; IRAF software packages distributed by the National Optical Astronomy Observatories, which are operated by the Association of Universities for Research in Astronomy, Inc., under cooperative agreement with the National Science Foundation; and the R software package (R Core Team 2014).

Facility: *Magellan*(M2FS).

REFERENCES

Aldenius, M., Tanner, J. D., Johansson, S., Lundberg, H., & Ryan, S. G. 2007, A&A, 461, 767
Aoki, W., Beers, T. C., Christlieb, N., et al. 2007a, ApJ, 655, 492
Aoki, W., Honda, S., Beers, T. C., et al. 2005, ApJ, 632, 611
Aoki, W., Honda, S., Sadakane, K., & Arimoto, N. 2007b, PASJ, 59, L15
Aoki, W., Tominaga, N., Beers, T. C., Honda, S., & Lee, Y. S. 2014, Sci, 345, 912
Arcones, A., & Thielemann, F.-K. 2013, JPhG, 40, 013201
Argast, D., Samland, M., Thielemann, F.-K., & Qian, Y.-Z. 2004, A&A, 416, 997
Asplund, M., Grevesse, N., Sauval, A. J., & Scott, P. 2009, ARA&A, 47, 481
Bailey, J. I., Mateo, M. L., Bagish, A. P., Crane, J. D., & Slater, C. T. 2012, Proc. SPIE, 8446, 84465G
Barklem, P. S., Christlieb, N., Beers, T. C., et al. 2005, A&A, 439, 129
Bechtol, K., Drlica-Wagner, A., Balbinot, E., et al. 2015, ApJ, 807, 50
Bedell, M., Meléndez, J., Bean, J. L., et al. 2014, ApJ, 795, 23
Beers, T. C., & Christlieb, N. 2005, ARA&A, 43, 531
Biémont, É, Blagoev, K., Engström, L., et al. 2011, MNRAS, 414, 3350
Booth, A. J., Blackwell, D. E., Petford, A. D., & Shallis, M. J. 1984, MNRAS, 208, 147
Bromm, V., & Larson, R. B. 2004, ARA&A, 42, 79
Bromm, V., & Loeb, A. 2003, Natur, 425, 812
Brown, T. M., Tumlinson, J., Geha, M., et al. 2012, ApJL, 753, L21
Carollo, D., Beers, T. C., Bovy, J., et al. 2012, ApJ, 744, 195
Castelli, F., & Kurucz, R. L. 2003, Proc. IAU Symp. 210, Modelling of Stellar Atmospheres, ed. N. Piskunov et al. (San Francisco, CA: ASP), A20
Cayrel, R., Hill, V., Beers, T. C., et al. 2001, Natur, 409, 691
Cescutti, G., Romano, D., Matteucci, F., Chiappini, C., & Hirschi, R. 2015, A&A, 577, A139
Christlieb, N., Beers, T. C., Barklem, P. S., et al. 2004, A&A, 428, 1027
Cohen, J. G., & Huang, W. 2010, ApJ, 719, 931
Cooke, R. J., & Madau, P. 2014, ApJ, 791, 116
Cowan, J. J., McWilliam, A., Sneden, C., & Burris, D. L. 1997, ApJ, 480, 246
Creevey, O. L., Thévenin, F., Boyajian, T. S., et al. 2012, A&A, 545, A17
Demarque, P., Woo, J.-H., Kim, Y.-C., & Yi, S. K. 2004, ApJS, 155, 667
Den Hartog, E. A., Lawler, J. E., Sneden, C., & Cowan, J. J. 2003, ApJS, 148, 543
Den Hartog, E. A., Lawler, J. E., Sneden, C., & Cowan, J. J. 2006, ApJS, 167, 292
Den Hartog, E. A., Lawler, J. E., Sobeck, J. S., Sneden, C., & Cowan, J. J. 2011, ApJS, 194, 35
Diehl, H. T., Abbott, T. M. C., Annis, J., et al. 2014, Proc. SPIE, 9149, 91490V
Drlica-Wagner, A., Bechtol, K., Rykoff, E. S., et al. 2015, ApJ, 813, 109
Feltzing, S., Eriksson, K., Kleyna, J., & Wilkinson, M. I. 2009, A&A, 508, L1
François, P., Monaco, L., Bonifacio, P., et al. 2015, A&A, submitted (arXiv:1510.05401)
Frebel, A., & Bromm, V. 2012, ApJ, 759, 115
Frebel, A., Casey, A. R., Jacobson, H. R., & Yu, Q. 2013, ApJ, 769, 57
Frebel, A., Christlieb, N., Norris, J. E., et al. 2006, ApJ, 652, 1585
Frebel, A., Christlieb, N., Norris, J. E., et al. 2007, ApJL, 660, L117
Frebel, A., Simon, J. D., Geha, M., & Willman, B. 2010, ApJ, 708, 560
Frebel, A., Simon, J. D., & Kirby, E. N. 2014, ApJ, 786, 74
Fujimoto, S.-i., Nishimura, N., & Hashimoto, M.-a. 2008, ApJ, 680, 1350
Geringer-Sameth, A., Walker, M. G., Koushiappas, S. M., et al. 2015, PhRvL, 115, 081101
Gilmore, G., Norris, J. E., Monaco, L., et al. 2013, ApJ, 763, 61
Goriely, S., Bauswein, A., & Janka, H.-T. 2011, ApJL, 738, L32
Hansen, T., Andersen, J., Nordström, B., Buchhave, L. A., & Beers, T. C. 2011, ApJL, 743, L1
Hansen, T., Hansen, C. J., Christlieb, N., et al. 2015a, ApJ, 807, 173
Hansen, T. T., Andersen, J., Nordström, B., et al. 2015b, A&A, 583, A49
Hansen, T. T., Andersen, J., Nordström, B., et al. 2015c, A&A, in press (arXiv:1511.08197)
Hayek, W., Wiesendahl, U., Christlieb, N., et al. 2009, A&A, 504, 511
Hill, V., Plez, B., Cayrel, R., et al. 2002, A&A, 387, 560
Hotokezaka, K., Piran, T., & Paul, M. 2015, NatPh, 11, 1042
Ishigaki, M. N., Aoki, W., Arimoto, N., & Okamoto, S. 2014a, A&A, 562, A146
Ishigaki, M. N., Tominaga, N., Kobayashi, C., & Nomoto, K. 2014b, ApJL, 792, L32
Ishimaru, Y., & Wanajo, S. 1999, ApJL, 511, L33
Ishimaru, Y., Wanajo, S., & Prantzos, N. 2015, ApJL, 804, L35
Ivans, I. I., Simmerer, J., Sneden, C., et al. 2006, ApJ, 645, 613
Ivarsson, S., Litzén, U., & Wahlgren, G. M. 2001, PhyS, 64, 455
Jablonka, P., North, P., Mashonkina, L., et al. 2015, A&A, 583, A67
Ji, A. P., Frebel, A., Chiti, A., & Simon, J. D. 2015a, Natur, submitted (arXiv:1512.01558)
Ji, A. P., Frebel, A., Simon, J. D., & Geha, M. 2015b, ApJ, 817, 41
Johnson, C. I., McWilliam, A., & Rich, R. M. 2013, ApJL, 775, L27
Johnson, J. A. 2002, ApJS, 139, 219
Johnson, J. A., & Bolte, M. 2002, ApJ, 579, 616
Kasen, D., Fernández, R., & Metzger, B. D. 2015, MNRAS, 450, 1777
Kirby, E. N., Martin, C. L., & Finlator, K. 2011, ApJL, 742, L25
Koch, A., Feltzing, S., Adén, D., & Matteucci, F. 2013, A&A, 554, A5
Koch, A., McWilliam, A., Grebel, E. K., Zucker, D. B., & Belokurov, V. 2008, ApJL, 688, L13
Koch, A., & Rich, R. M. 2014, ApJ, 794, 89
Komiya, Y., Yamada, S., Suda, T., & Fujimoto, M. Y. 2014, ApJ, 783, 132
Koposov, S. E., Belokurov, V., Torrealba, G., & Evans, N. W. 2015a, ApJ, 805, 130
Koposov, S. E., Casey, A. R., Belokurov, V., et al. 2015b, ApJ, 811, 62
Kramida, A., Ralchenko, Y., Reader, J. & the NIST ASD Team 2015, NIST Atomic Spectra Database (v. 5.3), online: http://physics.nist.gov/asd
Kratz, K.-L., Farouqi, K., Pfeiffer, B., et al. 2007, ApJ, 662, 39
Kurucz, R. L., & Bell, B. 1995, Kurucz CD-ROM (Cambridge, MA: Smithsonian Astrophysical Observatory)
Lai, D. K., Lee, Y. S., Bolte, M., et al. 2011, ApJ, 738, 51
Lawler, J. E., Bonvallet, G., & Sneden, C. 2001a, ApJ, 556, 452
Lawler, J. E., & Dakin, J. T. 1989, JOSAB, 6, 1457
Lawler, J. E., Den Hartog, E. A., Sneden, C., & Cowan, J. J. 2006, ApJS, 162, 227
Lawler, J. E., Guzman, A., Wood, M. P., Sneden, C., & Cowan, J. J. 2013, ApJS, 205, 11
Lawler, J. E., Sneden, C., Cowan, J. J., Ivans, I. I., & Den Hartog, E. A. 2009, ApJS, 182, 51
Lawler, J. E., Wickliffe, M. E., Cowley, C. R., & Sneden, C. 2001b, ApJS, 137, 341
Lawler, J. E., Wickliffe, M. E., den Hartog, E. A., & Sneden, C. 2001c, ApJ, 563, 1075
Lawler, J. E., Wood, M. P., Den Hartog, E. A., et al. 2014, ApJS, 215, 20
Lawler, J. E., Wyart, J.-F., & Blaise, J. 2001d, ApJS, 137, 351
Lee, D. M., Johnston, K. V., Tumlinson, J., Sen, B., & Simon, J. D. 2013a, ApJ, 774, 103
Lee, Y. S., Beers, T. C., Masseron, T., et al. 2013b, AJ, 146, 132
Li, R., Chatelain, R., Holt, R. A., et al. 2007, PhyS, 76, 577

Ljung, G., Nilsson, H., Asplund, M., & Johansson, S. 2006, A&A, 456, 1181
Mateo, M., Bailey, J. I., Crane, J., et al. 2012, Proc. SPIE, 8446, 84464Y
Mathews, G. J., Bazan, G., & Cowan, J. J. 1992, ApJ, 391, 719
Matteucci, F., Romano, D., Arcones, A., Korobkin, O., & Rosswog, S. 2014, MNRAS, 438, 2177
McConnachie, A. W. 2012, AJ, 144, 4
McWilliam, A. 1998, AJ, 115, 1640
McWilliam, A., Preston, G. W., Sneden, C., & Searle, L. 1995, AJ, 109, 2757
Metzger, B. D., Martínez-Pinedo, G., Darbha, S., et al. 2010, MNRAS, 406, 2650
Navarro, J. F., Frenk, C. S., & White, S. D. M. 1996, ApJ, 462, 563
Nilsson, H., Ljung, G., Lundberg, H., & Nielsen, K. E. 2006, A&A, 445, 1165
Nishimura, N., Takiwaki, T., & Thielemann, F.-K. 2015, ApJ, 810, 109
Norris, J. E., Gilmore, G., Wyse, R. F. G., Yong, D., & Frebel, A. 2010a, ApJL, 722, L104
Norris, J. E., Yong, D., Bessell, M. S., et al. 2013, ApJ, 762, 28
Norris, J. E., Yong, D., Gilmore, G., & Wyse, R. F. G. 2010b, ApJ, 711, 350
Palmeri, P., Fischer, C. F., Wyart, J.-F., & Godefroid, M. R. 2005, MNRAS, 363, 452
Pignatari, M., Gallino, R., Meynet, G., et al. 2008, ApJL, 687, L95
Placco, V. M., Frebel, A., Beers, T. C., & Stancliffe, R. J. 2014, ApJ, 797, 21
Prada, F., Klypin, A. A., Cuesta, A. J., Betancort-Rijo, J. E., & Primack, J. 2012, MNRAS, 423, 3018
Qian, Y.-Z., & Wasserburg, G. J. 2007, PhR, 442, 237
R Core Team 2014, R: A Language and Environment for Statistical Computing (Vienna: R Foundation for Statistical Computing) URL: http://www.R-project.org/
Raiteri, C. M., Busso, M., Picchio, G., Gallino, R., & Pulone, L. 1991, ApJ, 367, 228
Ramirez-Ruiz, E., Trenti, M., MacLeod, M., et al. 2015, ApJL, 802, L22
Ritter, J. S., Sluder, A., Safranek-Shrader, C., Milosavljević, M., & Bromm, V. 2015, MNRAS, 451, 1190
Roederer, I. U. 2009, AJ, 137, 272
Roederer, I. U. 2013, AJ, 145, 26
Roederer, I. U., Cowan, J. J., Karakas, A. I., et al. 2010, ApJ, 724, 975
Roederer, I. U., Cowan, J. J., Preston, G. W., et al. 2014a, MNRAS, 445, 2946
Roederer, I. U., & Kirby, E. N. 2014, MNRAS, 440, 2665
Roederer, I. U., Kratz, K.-L., Frebel, A., et al. 2009, ApJ, 698, 1963
Roederer, I. U., & Lawler, J. E. 2012, ApJ, 750, 76
Roederer, I. U., Lawler, J. E., Sneden, C., et al. 2008a, ApJ, 675, 723
Roederer, I. U., Mateo, M., Bailey, J. I., et al. 2016, MNRAS, 455, 2417
Roederer, I. U., Preston, G. W., Thompson, I. B., et al. 2014b, AJ, 147, 136
Roederer, I. U., Preston, G. W., Thompson, I. B., Shectman, S. A., & Sneden, C. 2014c, ApJ, 784, 158
Ruffoni, M. P., Den Hartog, E. A., Lawler, J. E., et al. 2014, MNRAS, 441, 3127
Ryan, S. G., Aoki, W., Norris, J. E., & Beers, T. C. 2005, ApJ, 635, 349
Sadakane, K., Arimoto, N., Ikuta, C., et al. 2004, PASJ, 56, 1041
Shen, S., Cooke, R. J., Ramirez-Ruiz, E., et al. 2015, ApJ, 807, 115
Shetrone, M., Venn, K. A., Tolstoy, E., et al. 2003, AJ, 125, 684
Shetrone, M. D., Côté, P., & Sargent, W. L. W. 2001, ApJ, 548, 592
Simon, J. D., Drlica-Wagner, A., Li, T. S., et al. 2015, ApJ, 808, 95
Simon, J. D., Frebel, A., McWilliam, A., Kirby, E. N., & Thompson, I. B. 2010, ApJ, 716, 446
Siqueira Mello, C., Spite, M., Barbuy, B., et al. 2013, A&A, 550, A122
Smith, B. D., Wise, J. H., O'Shea, B. W., Norman, M. L., & Khochfar, S. 2015, MNRAS, 452, 2822
Sneden, C., Cowan, J. J., & Gallino, R. 2008, ARA&A, 46, 241
Sneden, C., Cowan, J. J., Lawler, J. E., et al. 2003, ApJ, 591, 936
Sneden, C., Lawler, J. E., Cowan, J. J., Ivans, I. I., & Den Hartog, E. A. 2009, ApJS, 182, 80
Sneden, C., McWilliam, A., Preston, G. W., et al. 1996, ApJ, 467, 819
Sneden, C., Preston, G. W., McWilliam, A., & Searle, L. 1994, ApJL, 431, L27
Sneden, C. A. 1973, PhD thesis, Univ. Texas
Sobeck, J. S., Kraft, R. P., Sneden, C., et al. 2011, AJ, 141, 175
Sobeck, J. S., Lawler, J. E., & Sneden, C. 2007, ApJ, 667, 1267
Starkenburg, E., Shetrone, M. D., McConnachie, A. W., & Venn, K. A. 2014, MNRAS, 441, 1217
Tafelmeyer, M., Jablonka, P., Hill, V., et al. 2010, A&A, 524, A58
Truran, J. W., Cowan, J. J., Pilachowski, C. A., & Sneden, C. 2002, PASP, 114, 1293
Tsujimoto, T., Ishigaki, M. N., Shigeyama, T., & Aoki, W. 2015, PASJ, 67, L3
Tsujimoto, T., & Shigeyama, T. 2014, A&A, 565, L5
Udry, S., Mayor, M., Maurice, E., et al. 1999, in ASP Conf. Ser. 185, Precise Stellar Radial Velocities, ed. J. B. Hearnshaw & C. D. Scarfe (San Francisco, CA: ASP), 383
Umeda, H., & Nomoto, K. 2005, ApJ, 619, 427
van de Voort, F., Quataert, E., Hopkins, P. F., Kereš, D., & Faucher-Giguère, C.-A. 2015, MNRAS, 447, 140
Venn, K. A., Shetrone, M. D., Irwin, M. J., et al. 2012, ApJ, 751, 102
Walker, M. G., Mateo, M., Olszewski, E. W., et al. 2015, ApJ, 808, 108
Wallner, A., Faestermann, T., Feige, J., et al. 2015, NatCo, 6, 5956
Wanajo, S., Tamamura, M., Itoh, N., et al. 2003, ApJ, 593, 968
Webster, D., Frebel, A., & Bland-Hawthorn, J. 2016, ApJ, in press
Westmeier, T., Staveley-Smith, L., Calabretta, M., et al. 2015, MNRAS, 453, 338
Wickliffe, M. E., Lawler, J. E., & Nave, G. 2000, JQSRT, 66, 363
Wickliffe, M. E., Salih, S., & Lawler, J. E. 1994, JQSRT, 51, 545
Wood, M. P., Lawler, J. E., Sneden, C., & Cowan, J. J. 2013, ApJS, 208, 27
Wood, M. P., Lawler, J. E., Sneden, C., & Cowan, J. J. 2014, ApJS, 211, 20
Woosley, S. E., & Hoffman, R. D. 1992, ApJ, 395, 202